Optimizing Reliability of PV based Microgrid by Integrating Fuel Cell

Rashmi R. Swain[1][0000-0001-6139-2384], Pradyumna K. Behera[2][0000-0001-6196-4987], Indrajit Sarkar[3][0000-0001-7212-4799], and Monalisa Pattnaik[4][0000-0003-0309-7111]

Department of Electrical Engineering,
National Institute of Technology, Rourkela, Odisha, IN-769008
[1]rrashmi898@gmail.com, [2]pkb.vssut14@gmail.com,
[3]sarkari@nitrkl.ac.in, [4]pattnaikm@nitrkl.ac.in

Abstract. In the last few decades, solar photovoltaic (PV) based DC microgrids (MG) have become increasingly popular in applications such as electric vehicle (EV) charging, domestic and commercial power supplies etc. However, due to the uncertainty in solar power generation, the reliability of such systems is low for standalone applications, and hence, energy storage systems (ESS) are necessary to maintain power flow when power generation is not sufficient due to low irradiance or during night time. In solutions where batteries are used as ESS is bulky, heavy, and slow in response due to low power density, and therefore, not suitable for applications requiring fast transient response. Fuel cell (FC) technology on the other hand has become a promising non-conventional energy source featuring both high energy density and power availability, though has slow dynamic response. Furthermore, the compactness and portable feature of FC enable it to to use in almost every field that uses battery as ESS (BESS). In this work, an existing DC MG consisting of solar PV, BESS, and DC load is considered. The solar PV and the battery are connected to the MG DC bus via buck and bi-directional DC-DC converters respectively, whereas the FC is integrated using a boost converter. The Perturb and Observe (P&O) maximum power point tracking (MPPT) algorithm is implemented to track the maximum power point (MPP) of both PV and FC. Here, the DC bus voltage is maintained at 48 V by the bi-directional converter using a Proportional-Integral (PI) controller. This work highlights the MPPT of FC and the integration of solar PV, BESS, and FC to the DC MG leading to cleaner and more efficient energy solution.

Keywords: Fuel cell, PEMFC, PV array, Microgrid, Perturb & Observe MPPT algorithm, DC bus voltage regulation.

1 Introduction

With the unprecedented demand for energy in modern society, various challenges posed due to fossil fuel depletion as well as several environmental concerns, significant research emphasis is on the integration of renewable energy sources (RES)

such as solar PV, wind, biomass, etc. and adoption of microgrid (MG) technologies [1, 2]. The transition from conventional power systems to solar microgrid (SMG) reflects a global push towards sustainable power generation practices. A MG is a localized and often decentralized network of electrical sources, such as solar PVs, BESSs, loads, and sometime FCs operating independently to generate, distribute, and control the power flow within a specific geographic area or community [3, 4]. The purpose of a MG is to provide reliable and affordable energy to a specific area or community while reducing the reliance on the electrical grid. However, the MG integrated with RESs suffers from power fluctuations due to the sporadic nature of RES and the intermittency is a challenge for the grid operators and energy planners to balance the supply and demand of electricity in real-time [5].

To address the intermittency issue different types of RES with complementary characteristics are combined in a hybrid system. For example, wind and solar PV systems are hybridized to produce more consistent and reliable energy output. Another approach is to use energy storage devices (ESDs) such as batteries, pumped hydro storage, flywheels, etc. to store excess energy and release it whenever needed [3, 5, 6]. In a standalone MG, the ESDs play a critical role in regulating and smoothing out instantaneous power fluctuations, ensuring a reliable and stable energy supply. Among several ESDs, the battery is a widely preferred option due to its high specific energy density [7]. However, the hybrid MGs have several drawbacks such as partial shading in solar generation, variations in wind power generation due to low or extremely wind speeds. Furthermore, the extensive use of batteries as ESD has several drawbacks such as low energy conversion efficiency, short lifespan due to rapid charging and discharging cycles, complex control, high upfront and recurring expenses, bulky, heavy, and potential for chemical hazards.

FC technology on the other hand has emerged as one of the clean and reliable power source with minimal dependency on weather condition and hence nearly generate electrical power without any interruption. Therefore, the use of Hydrogen (H_2) for power generation is getting more attention as it is considered to be superior due to its high energy conversion efficiency and long-term storage without any significant leakage [8]. The hydrogen-based proton exchange membrane fuel cell (PEMFC) due to its remarkable specific energy density stands out as a prospective power source for the future. The high reliability, efficiency and energy density of FC makes it an eco-friendly and viable choice for integration into MGs. The power generation and energy storage using a FC combination needs to be operated in a very controlled manner depending on storage requirements, power flow management and load transients [8]. Furthermore, hydrogen-based FC has unrivaled potential to be the green power source of the future and become a key enabler for the global transition towards carbon-intensive economies. However, the integration of FC systems with the conventional electrical infrastructure as well as MG is little explored.

In MG applications, the integration of multiple energy sources and their power extractions is achieved by implementing MPPT algorithms to individual

power sources [9–11]. For example, as in solar PV power extraction, a DC-DC converter with MPPT control is implemented, a similar MPPT technique needs to be employed for FC power sources when it is integrated with an MG. However, to regulate the DC bus voltage, a BESS needs to be integrated using a bidirectional DC-DC converter in conjunction with the MPPT converters [12]. Here, the dc bus voltage is maintained within tolerable limits using a closed-loop control [13]. Moreover, hydrogen-based FC has unrivalled potential to be the green power source of the future and become a key enabler for the global transition towards carbon-intensive economies. However, the integration of FC systems with the conventional electrical infrastructure as well as MG is little explored. Therefore, it is concluded that there is a constant thrust in the area for implementing hybrid systems comprising solar PV, FC and BESS for MG applications.

In this work, the MPP operation of solar PV and FC is implemented for a PV-FC based stadalone DC MG with DC bus voltage regulation using BESS equipped with a bi-directional DC-DC converter. The work presented here is as follows, section 2 deals with the system modeling of solar PV, BESS, and PEMFC; in section 3 various control strategies of the sources and DC bus voltage regulations are presented; and section 4 discusses the result analysis of simulation studies. Finally, section 5 presents the conclusion.

2 System Description and Modelling

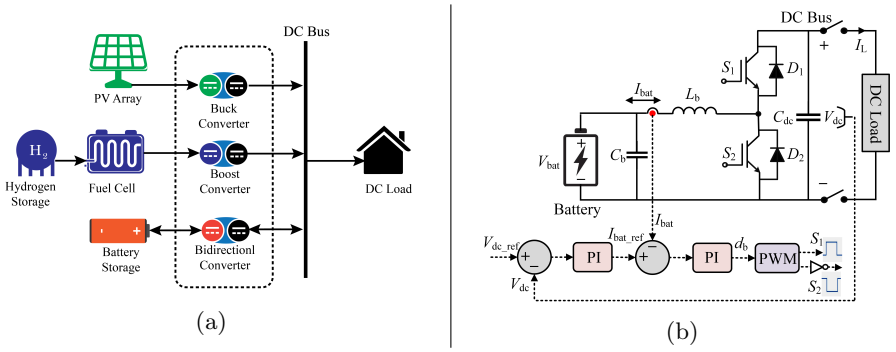

Fig. 1: (a)Single line diagram of PV-FC based DC MG, (b) DC bus voltage control using bidirectional DC-DC converter.

The single-line diagram of the PV-FC fed standalone DC MG is represented in Fig. 1a. Two DERs namely PV and FC are utilized to feed power to the load. The system also includes a BESS which works together to store and distribute energy to the load. DC-DC converters play a crucial role in regulating the DC voltage levels within the MG. To enhance system efficiency, it is essential to utilize an effective MPPT algorithm for both the solar PV and FC systems. The PV module is connected to the DC bus using a DC-DC buck converter, while the

FC unit is interfaced to the DC bus via a boost converter. To maintain power balance and regulate the DC bus at the desired level, the BESS is connected using a non-isolated bidirectional converter. By incorporating a hydrogen-based source FC, the overall burden on the backup system (i.e. BESS) during the absence of PV reduces. Furthermore, for proper design and simulation of the entire system, modelling of PV, BESS and FC is important which is presented in the following subsections.

2.1 Solar PV Modelling

The single-diode model with series and parallel resistances is adapted [14] for modelling the PV cell. The dynamic equation that governs the output current (I) of a PV cell can be obtained as follows.

$$I = I_{ph} - I_o \left[\exp\left(\frac{V + IR_{se}}{N_s V_t} - 1\right)\right] - \frac{V + IR_{se}}{R_{sh}} \tag{1}$$

Where, I is the output current of the solar PV module and V is the terminal voltage, I_{ph} is the photo-generated current also considered as a constant current source, I_o is the reverse saturation current of diode, R_{se} is the series resistance, R_{sh} is the parallel resistance, N_s is the total no of cells connected in series inside the module, V_t is the junction thermal equivalent voltage and can be expressed as $V_t = \frac{kAT}{q}$, in which k is the Boltzmann's constant i.e. $1.38 \times 10^{23} J/K$, q is the charge of electron i.e. $1.602 \times 10^{-19} C$, and A is the ideality constant of diode.

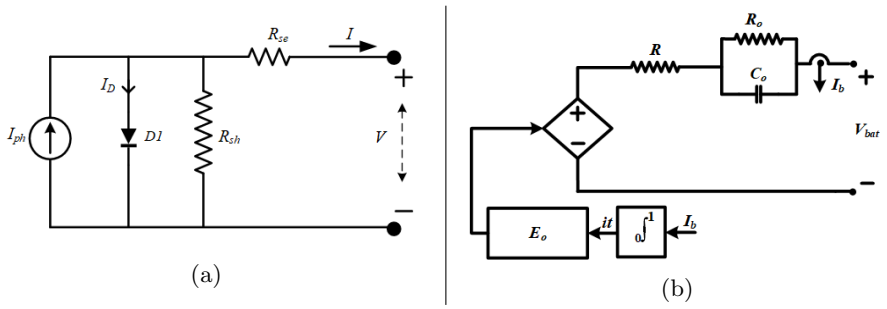

Fig. 2: Equivalent Circuit: (a) single diode model of PV, (b) Battery cell.

2.2 BESS Modeling

The electrical equivalent circuit representation of single BESS cell is depicted in Fig. 2b and the equation for terminal voltage can be modelled as [15].

$$V_{bat} = E_0 - K\frac{Q}{Q - it}.it - R.i + A\exp(-B.it) - K\frac{Q}{Q - it}.i^* \tag{2}$$

where, V_{bat} is battery voltage (V), E_o is the ideal no-load battery voltage (V), K is the Polarization voltage, Q is the battery capacity (Ah), $it = \int i.dt$ is the

actual available battery charge (Ah); A is the exponential zone amplitude (V); B is time constant inverse (Ah^{-1}); R is the internal resistance of source (Ω); I_{bat} is battery output current (A); i^* is the filtered current.

2.3 FC Modelling

The PEMFC is a form of electrochemical cell that uses chemical reactions to turn hydrogen and oxygen into electricity, heat, and water. There are two types of models exists for FC i.e. the dynamic gas transport model (DGTM) and the polarisation curve model (PCM). This work solely focuses on PCM based modelling as it is less complex and easy to implement. PEMFC operation is based on the principle of electrochemical interactions which comprises of a proton exchange membrane isolating the anode from the cathode. The dynamic model can be obtained from the equivalent circuit [16] and the output voltage of a single FC unit is presented by (Fig.3b) (Eq.3). The relation between terminal

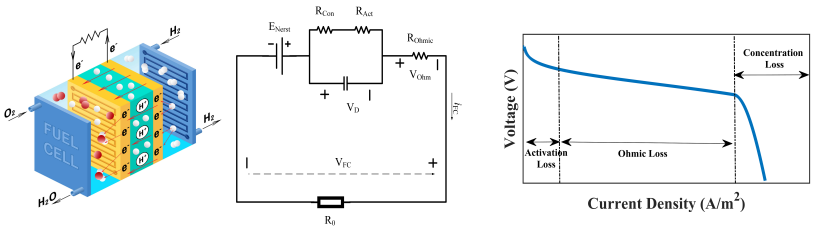

(a) (b) (c)

Fig. 3: PEMFC (a) Graphical illustration [17], (b) Equivalent circuit, (c) Polarization curve.

voltage and current density of a FC known as the polarization curve (Fig. 3c) provides the voltage output at any given current density. There are three specific regions in a polarization curve i.e. activation loss region, ohmic loss region, and concentration loss region. Activation loss (Eq. 5) region indicates the drop or loss due to activation of the cell to overcome the energy barrier, ohmic loss (Eq. 6) region depicts drop in the cell voltage as a result of built-in resistance of membrane and electrodes while concentration loss (Eq. 6) occurs due to mass transport of charges inside the cell and proportional to current density of the cell. One can ignore the loss due to mass transport if the power density is low [16]. The polarization curve also interprets how much power can be generated from a certain amount of fuel supply. The mathematical equation of FC is given below [18].

$$V_{FC} = (E_{Nerst} - V_{act} - V_{Ohm} - V_{con}) \tag{3}$$

where, E_{Nerst} can be given as

$$E_{Nerst} = \frac{1}{2F}\left[\Delta G - \Delta S\left(T - T_{ref}\right) + RT\left(\ln P_{H_2} + \frac{\ln P_{O_2}}{2}\right)\right] \tag{4}$$

The activation loss is produced by the rapid chemical reaction happening on the active surface of the electrodes and can be estimated as follows (Eq.5).

$$V_{act} = \zeta_1 + \zeta_2 T + \zeta_3 T[\ln(C_{O_2})] + \zeta_4 T[\ln(i)] \tag{5}$$

where, $\zeta_1, \zeta_2, \zeta_3, \zeta_4$ are the constants which can be obtained by experimental method or from manufacturer datasheet. Other constant parameters required to model the device are referred from [16]. The Ohmic loss and concentration loss are depicted in Eq.6.

$$V_{Ohm} = i\left(R_M + R_c\right), V_{con} = B\ln\left(1 - \frac{J}{J_{max}}\right) \tag{6}$$

where, equivalent resistance between membrane and electrode surface contact is R_c, equivalent impedance of membrane is R_M, current density at electrode surface is J and concentration polarization factor is B respectively.

3 Control Aspects of PV-FC-BESS fed DC MG

The design of a suitable controller plays a crucial role in coordinating and controlling the power electronic converters in an autonomous DC MG. It ensures the efficient utilization of power generated by DERs to meet the demand while maintaining the stability and reliability of the MG. The control of the converters of the solar PV and FC is optimized to achieve the maximum power output. MPPT algorithms are used to optimize power extraction irrespective of unpredictable conditions i.e., ambient temperature and intensity of solar irradiation in PVs, flow rate (fuel/air) in FCs [19]. The DC-DC bidirectional converter of the BESS operates in charging/discharging mode depending on the generation and demand disparity and also maintains a constant DC bus voltage. The next subsections describe PV and FC MPPT as well as DC bus voltage regulation operations sequentially. The charging mode is activated when the generation exceeds the demand, and the discharging mode is activated when the demand exceeds the generation. By maintaining a balance between the power generated and the power consumed, the PMS ensures that the MG operates efficiently and reliably.

3.1 MPPT of Solar PV System

The P&O method is widely used for maximum power extraction and involves regularly adjusting the duty ratio (D) of the DC-DC converter by measuring the output current (I_{PV}) and voltage (V_{PV}) of the panel, and thereby calculating

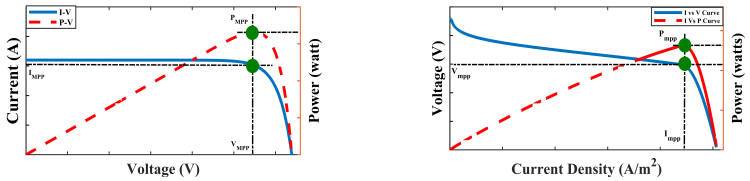

(a) (b)

Fig. 4: (a) PV module *I-V* & *P-V* characteristics, (b) FC stack *V-I* & *P-I* characteristics.

the power output (P_{PV}). After determining the power output, the slope of the P-V curve (Fig. 4a) or the operating region is checked to determine whether it is a current source or voltage source region [20]. Then, the duty ratio D is adjusted in a way that brings the operating point closer to the MPP. By introducing a small perturbation to the duty cycle, a new operating point is obtained. If P_{PV} and V_{PV} increases with the duty cycle adjustment, the operating point is on the left side of the MPP, and further adjustments in the same direction will move it towards the top of the hill (i.e. MPP). If P_{PV} decreases with duty cycle change and V_{PV} either increases or decreases, the direction of the perturbation needs to be changed. Based on changes in V_{PV} and P_{PV}, the operating point has moved up or down the hill on either side of the MPP and further perturbed to reach the MPP. The algorithm is illustrated in Fig.5a and the detailed mathematical relationships are delineated in [10], [21].

3.2 MPPT of FC Stack

P&O MPPT tracking algorithm for FC unit is slightly different from previously motioned P&O approach for solar PV unit [22]. In Fig.4b, the dotted line represents the current vs power characteristic and the solid line represents the polarization curve. By superimposing both the curves, the maximum power output and corresponding voltage and current values can be obtained [19]. Rather than perturbing voltage, the algorithm perturbs the FC current and the resulting change in power is observed. If the power change is positive, it indicates that the operating point has moved toward the MPP. Consequently, the operating current is further adjusted in the same direction. To the contrary, if the power change is negative, it conveys that the operating point has moved away from the MPP and thus the direction of the current adjustment is reversed. The flowchart of P&O algorithm for FC is illustrated in Fig.5b.

3.3 DC Bus Voltage Regulation

To ensure stable operation of the system, the DC bus voltage should be maintained constant regardless of operational conditions. By achieving this, the DC MG can effectively adapt to changes in power generation/demand from the DERs and load while ensuring proper charging/discharging of the BESS. The charging

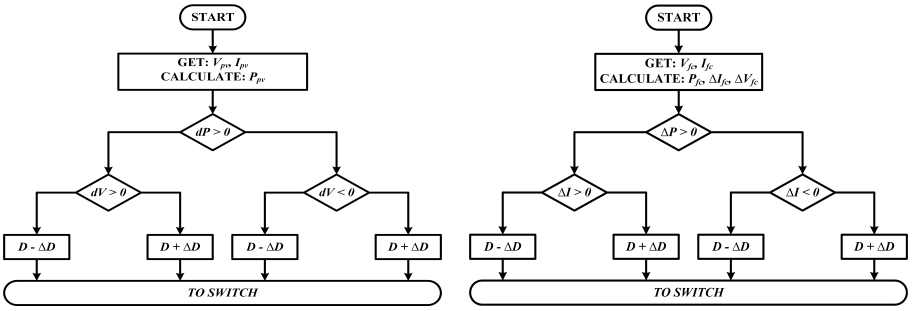

(a) (b)

Fig. 5: Flowchart of P&O MPPT control (a)PV Module, (b) PEMFC stack.

Table 1: PV-FC based Standalone MG parameters

DC bus voltage = 48 V, Load power = 2.56 kW Switching Frequency (f_{sw}) = 20 kHz, Sampling Time (T_s) = 1 μs
PV Module Parameters at STC
PV Array: 1.63 kW,V_{oc}= 35.55 V, I_{sc}= 7.91 A, V_{mp} = 28.04 V, I_{mp}= 7.31 A N_P per string = 2, N_{se} per string = 4,N_s per module= 60 Buck Converter: L_{PV} = 1 mH, C_{PV} = C_{dc1} = 1000 μF
Fuel Cell Parameters
Fuel cell stack: 42 V, 1.3 kW, V_{mp} = 30.23 V, I_{mp} = 43 A, E_{Nerst} = 1.115 V Fuel flow rate = Air flow rate = 13 L/m, P_{fuel} = 1.5 bar, P_{air} = 1 bar Fuel Composition (H_2, O_2) = 99.95 %, 21 %, System Temperature (T) = 328 ^0K Boost Converter: L_{FC} = 1 mH, C_{dc2} = 1000 μF
Battery Parameters
Nominal Voltage = 24 V, Rated Capacity = 42 Ah, Initial SOC = 75 % Bidirectional Converter: L_{bat} = 1 mH, C_{bat} = 470 μF, C_{dc3} = 1000 μF

mode is activated when the generation exceeds the demand, and the discharging mode is activated when the demand exceeds the generation. Fig. 1b illustrates the cascaded double-loop control strategy of the bidirectional converter. The output reference of the voltage loop PI controller is used as the reference for the inductor current of the converter. The generated battery reference current is compared with the actual current. The error signal is fed through the PI controller for the generation of the duty ratio to obtain the switching pulse of the bidirectional buck-boost converter.

4 Simulation Results And Discussions

In this section, the simulation result and analysis of the standalone PV, FC integrated with the BESS is presented. The specifications of the complete system are provided in Table 1. The simulation results of the PV system operating under MPPT are depicted in Fig. 6. The simulation is carried out at two different irradiations (i.e. 1000 W/m^2 and 800 W/m^2). The PV system is initially operated

at an irradiation level of 1000 W/m^2 and the corresponding optimum power is 1.63 kW. At $t = 1.5$ s, the irradiation level suddenly drops to 800 W/m^2 resulting in the reduction of PV power to 1.32 kW (Fig. 6(b)). Due to the irradiation decrease, the PV voltage dips and the duty cycle settles at the new operating point retracing the MPP voltage as Fig. 6(a) and (c) and the corresponding PV current is shown in Fig. 6(d). It can inferred that the PV system tracks the MPP properly despite variation in irradiation. Similarly, the simulation results of the FC system operating under MPP are depicted in Fig. 7. It can be observed that the FC system is introduced at $t = 0.5$ s, the operating duty cycle, corresponding power, voltage and current are shown in Fig. 7(a), (b), (c) and (d) respectively. The maximum power tracked by the system using the P&O MPPT algorithm is 1.3 kW Fig. 7 (b).

After testing the individual MPPT operation of PV and FC systems, the power-

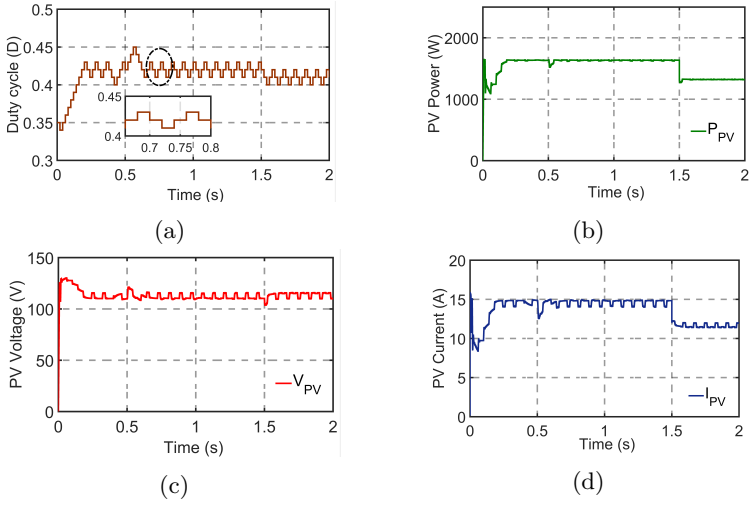

Fig. 6: MPPT results of PV array (a) Duty cycle (b) P_{PV} (c)V_{PV} (d) I_{PV}.

sharing operation of PV, FC integrated with BESS is verified. The system is tested under the normal power-sharing mode (i.e. $30\% \leq SOC \leq 90\%$). The corresponding simulation results are presented in Fig. 8. The power profiles of PV, FC, BESS and load unit during the entire operation are represented in Fig. 8(a). The PV, BESS, FC, and load currents are illustrated in Fig. 8 (b) followed by MG DC bus voltage and BESS %SOC in Fig. 8(c) and (d) respectively. Initially, the solar PV system interface with the BESS operates to meet the load requirement. From t = 0-0.5 s, the solar PV system generates the maximum power of 1.63 kW at irradiation of 1000 W/m^2 which is insufficient to meet the load requirement of 2.56 kW. Therefore, the battery supplies an additional 0.95 kW meeting the load demand and power loss of the converters. During this period, the BESS is in discharging mode and it can be observed that the BESS current profile tracks properly with its reference. The DC bus voltage is main-

tained at the rated value (i.e. 48 V). At $t = 0.5$ s, the FC system is introduced and the power extracted from it is 1.3 kW. The combined power of solar PV and FC is sufficient enough to meet the total load demand and the extra power available (100 W) is stored in the BESS. As already mentioned, at $t = 1.5$ s irradiance decreases to 800 W/m^2 and correspondingly due to drop in solar PV power generation, the BESS power is around zero and it remains in the float mode (i.e. the BESS current seems to be zero, but it is charging/discharging with a small power). During all these transients, the BESS current and DC bus voltage track their respective references satisfactorily having proper power sharing among the DERs, load and storage.

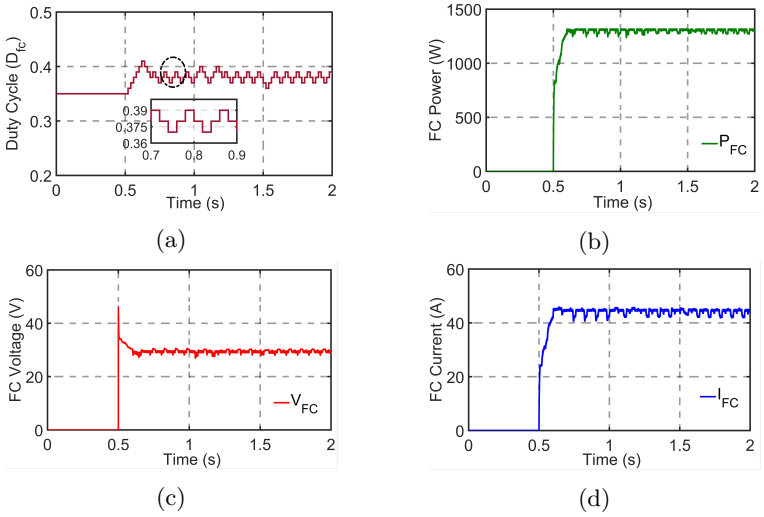

Fig. 7: MPPT results of FC Stack (a) Duty cycle (b)P_{FC} (c) V_{FC} (d) I_{FC}.

5 Conclusions

In this work, the successful integration of FC with existing DC MG is achieved with MPPT to extract maximum power, and tight regulation of DC bus voltage at 48 V using the BESS with bidirectional DC/DC converter. The dynamics of load sharing among different sources is also achieved within the MG which revealed the balanced sharing of power between the sources and load. Here, BESS played a critical role in this endeavour by storing the surplus power from different sources and releasing the deficit power to load on demand. Moreover, the FC MPPT optimised its power extraction and hence, maximized its contribution to the MG system. Also the resilience and adaptiveness of the system is observed in the outcomes. In summary, the seamless integration of FC contributed to a durable and efficient energy ecosystem, aligning with objectives of sustainable and reliable power systems.

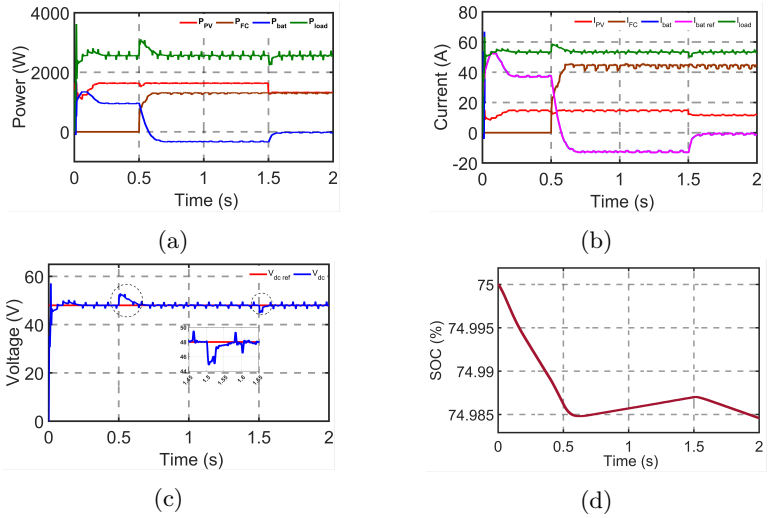

Fig. 8: DC MG with DC bus voltage regulation (a) P_{PV}, P_{FC}, P_{bat}, and P_{load} (b) I_{PV}, I_{FC}, I_{batref}, I_{bat} and I_{load} (c) V_{dc} and V_{dcref} (d) $\%SOC$ of BESS

References

1. J. Zheng, J. Du, B. Wang, J. J. Klemeš, Q. Liao, and Y. Liang, "A hybrid framework for forecasting power generation of multiple renewable energy sources," *Renewable and Sustainable Energy Reviews*, vol. 172, p. 113046, 2023.
2. J. Mishra, P. K. Behera, M. Pattnaik, and B. C. Babu, "A multi-agent petri net model power management strategy for wind–solar-battery driven dc microgrid," *Sustainable Energy Technologies and Assessments*, vol. 55, p. 102859, 2023.
3. P. K. Behera and M. Pattnaik, "Coordinated power management of a laboratory scale wind energy assisted lvdc microgrid with hybrid energy storage system," *IEEE Transactions on Consumer Electronics*, 2023.
4. M. Uddin, H. Mo, D. Dong, S. Elsawah, J. Zhu, and J. M. Guerrero, "Microgrids: A review, outstanding issues and future trends," *Energy Strategy Reviews*, vol. 49, p. 101127, 2023.
5. P. K. Behera and M. Pattnaik, "Power management of a laboratory scale wind-pv-battery based lvdc microgrid," in *2022 IEEE IAS Global Conference on Emerging Technologies (GlobConET)*. IEEE, 2022, pp. 509–514.
6. P. K. Behera, P. K. Piyush, and M. Pattnaik, "Design, sizing and implementation of a parallel active battery-supercapacitor based hybrid energy storage system," in *2023 International Conference on Power Electronics and Energy (ICPEE)*. IEEE, 2023, pp. 1–5.
7. J. Mishra, P. K. Behera, M. Pattnaik, and S. Samanta, "An efficient supervisory power management scheme for a wind–battery-assisted hybrid autonomous system," *IEEE Systems Journal*, vol. 17, no. 1, pp. 768–779, 2022.

8. M. Yue, H. Lambert, E. Pahon, R. Roche, S. Jemei, and D. Hissel, "Hydrogen energy systems: A critical review of technologies, applications, trends and challenges," *Renewable and Sustainable Energy Reviews*, vol. 146, p. 111180, 2021.
9. M. Kabalo, B. Blunier, D. Bouquain, and A. Miraoui, "State-of-the-art of dc-dc converters for fuel cell vehicles," in *2010 IEEE Vehicle Power and Propulsion Conference*. IEEE, 2010, pp. 1–6.
10. P. K. Behera, B. Mishra, and M. Pattnaik, "Geometrical interpretation of incremental conductance mppt algorithm for a stand-alone photovoltaic system," in *2021 Innovations in Power and Advanced Computing Technologies (i-PACT)*. IEEE, 2021, pp. 1–6.
11. B. Subudhi and R. Pradhan, "A comparative study on maximum power point tracking techniques for photovoltaic power systems," *IEEE transactions on Sustainable Energy*, vol. 4, no. 1, pp. 89–98, 2012.
12. W. Li and X. He, "Review of nonisolated high-step-up dc/dc converters in photovoltaic grid-connected applications," *IEEE Transactions on industrial electronics*, vol. 58, no. 4, pp. 1239–1250, 2010.
13. R. Gugulothu, B. Nagu, and D. Pullaguram, "Energy management strategy for standalone dc microgrid system with photovoltaic/fuel cell/battery storage," *Journal of Energy Storage*, vol. 57, p. 106274, 2023.
14. P. K. Behera and M. Pattnaik, "Design and control of dc–dc converters in a pv-based lvdc microgrid," *DC—DC Converters for Future Renewable Energy Systems*, pp. 1–29, 2022.
15. O. Tremblay, L.-A. Dessaint, and A.-I. Dekkiche, "A generic battery model for the dynamic simulation of hybrid electric vehicles," in *2007 IEEE vehicle power and propulsion conference*. Ieee, 2007, pp. 284–289.
16. J. Jia, Q. Li, Y. Wang, Y. Cham, and M. Han, "Modeling and dynamic characteristic simulation of a proton exchange membrane fuel cell," *IEEE Transactions on Energy Conversion*, vol. 24, no. 1, pp. 283–291, 2009.
17. https://andretti1.com/mechanics-hydrogen-fuel-cell/fuel-cell-diagram-vector-illustration.
18. J. Kim, S.-M. Lee, S. Srinivasan, and C. E. Chamberlin, "Modeling of proton exchange membrane fuel cell performance with an empirical equation," *Journal of the electrochemical society*, vol. 142, no. 8, p. 2670, 1995.
19. M. A. Masoum, H. Dehbonei, and E. F. Fuchs, "Theoretical and experimental analyses of photovoltaic systems with voltageand current-based maximum power-point tracking," *IEEE Transactions on energy conversion*, vol. 17, no. 4, pp. 514–522, 2002.
20. P. K. Behera, S. Das, and M. Pattnaik, "Performance comparison between bipolar and unipolar switching scheme for a single-phase inverter based stand-alone photovoltaic system," in *2019 IEEE 16th India Council International Conference (INDICON)*. IEEE, 2019, pp. 1–4.
21. P. K. Behera, R. R. Sahoo, and P. Ray, "Analysis of modified inc mppt technique with variable step for photovoltaic system," in *2017 International Conference on Energy, Communication, Data Analytics and Soft Computing (ICECDS)*. IEEE, 2017, pp. 541–546.
22. M. Büyük and M. İnci, "Improved drift-free p&o mppt method to enhance energy harvesting capability for dynamic operating conditions of fuel cells," *Energy*, vol. 267, p. 126543, 2023.